

# Synthesis and Magnetic Properties of One-Dimensional Zinc Nickel Oxide Solid Solution

Xiao Li Zhang, Ru Qiao, Ri Qiu, Yan Li, and Young Soo Kang\*

Department of Chemistry, Pukyong National University, 599-1 Daeyeon-3-dong, Namgu, Busan 608-737, Korea

Received: December 16, 2006; In Final Form: February 28, 2007

A novel facile method has been demonstrated for large-scale synthesis of zinc-oxide-based one-dimensional solid solution with a series percentage of nickel dopant. The obtained  $Zn_{1-x}Ni_xO$  nanorods were characterized by X-ray diffraction, transmission electron microscopy, selected area electron diffraction, and energy dispersed X-ray spectroscopy. The result shows that the obtained  $Zn_{1-x}Ni_xO$  nanorods are single crystalline with the  $Ni^{2+}$  dopants occupying tetrahedral  $Zn^{2+}$  cation sites of wurtzite ZnO. Moreover, the  $Zn_{1-x}Ni_xO$  nanorods exhibit robust high-Curie-temperature ( $T_C$ ) ferromagnetism at 300 K.

## Introduction

One-dimensional wurtzite-structured ZnO nanomaterials have attracted extensive interest because of the wide potential applications based on their optical and electric properties.<sup>1</sup> The direct band gap energy (3.37 eV) promises ZnO as an ideal candidate for low-voltage and short-wavelength electro-optical devices in electronics, optoelectronics, photovoltaics, and sensors. Fabricating one-dimensional nanoscaled crystal structures with designed electrical and optical properties is highly desired as beyond the controlled shapes for application as sensors, field-emitters, and spintronics.<sup>2</sup> Contemporaneously, on another research edge, led by the discovery of ferromagnetism in transition-metal-doped semiconductors, spintronics (spin-based electronics) has been deeply studied both theoretically and experimentally due to its enabling spin as well as the charge freedom of the carriers for new concept devices.<sup>3</sup> To present as practical spintronics devices, the materials must exhibit ferromagnetic ordering at high temperature. In the quest for materials with a high magnetic transition temperature, transition-metal-doped ZnO has emerged as a attractive candidate as it is theoretically predicted to be ferromagnetic at room temperature.<sup>3b,4</sup> In fact, as one of the II–VI semiconductors, ZnO is optically transparent and the direct wide band gap makes it an ideal candidate for the magneto-optical devices.<sup>5</sup> In addition, Dietl et al. suggested that  $Zn_{1-x}M_xO$  ( $M = Mn, Fe, Ni, Co$ ) exhibit a high transition temperature.<sup>3b</sup>

Practically, this system has been experimentally studied, however, room-temperature ferromagnetism has been reported in the vast majority of bulk materials, thin films, or colloids, etc.<sup>6</sup> ZnO-based one-dimensional dilute magnetic solid solutions (so-called dilute magnetic semiconductors, DMS) are of vital importance because they not only play an important role as the building blocks of electronic and spintronic devices in the bottom-up milestone but also provide excellent opportunities to study the effect of dimensionality and size on magnetism.<sup>7</sup> To date, little work has been done on the fabrication of one-dimensional nanostructured  $Zn_{1-x}M_xO$  through chemical vapor deposition (CVD) method, which has played as superior because it is quite effectiveness in producing a great amount of one-dimensional nanoscaled semiconductors.<sup>7,8</sup> Nevertheless, the CVD methods are evidently limited in homogeneous doping at the extreme vapor-phased experimental conditions.

Solution-phased synthetic schemes for the producing  $Zn_{1-x}M_xO$  isotropic quantum dots have been reported by Gamelin et al.<sup>9</sup> Very recently, Yang et al. first reported a solution-phased method for fabrication of  $Zn_{1-x}Co_xO$  nanowire by thermal decomposition of zinc acetate and cobalt(II) acetate in refluxing trioctylamine at 310 °C,<sup>10</sup> and Wong et al. reported a two-step solution-phased method for the synthesis of rod-shaped  $Zn_{1-x}Co_xO$  by introducing pure ZnO seeds as nucleation centers.<sup>11</sup> Herein, following our early work on nonsurfactant synthesis of one-dimensional ZnO nanomaterials,<sup>1d</sup> we present a simple and facile method of large-scale synthesis of a zinc-oxide-based one-dimensional solid solution with a series percentage of nickel dopant. Moreover, the synthetic process here also allows for the introduction of other transition metals such as Co and Mn, etc.

## Experimental Section

The synthesis of one-dimensional  $Zn_{1-x}Ni_xO$  solid solution is based on an alcoholysis process originally developed for ZnO nanocrystal preparation by Kang et al.<sup>1d</sup>  $Zn_{1-x}Ni_xO$  nanorods with a series of percentage of nickel dopant were synthesized by similar procedures. In a typical  $Zn_{1-x}Ni_xO$  nanorods synthesis, 4.95 mmol zinc acetate dihydrate ( $(C_2H_3O_2)_2Zn \cdot 2H_2O$ , 98+%, Aldrich) and 0.05 mmol nickel(II) acetate tetrahydrate ( $(C_2H_3O_2)_2Ni \cdot 4H_2O$ , 99.998%, Aldrich) were completely dissolved in 20 mL of methanol ( $CH_3OH$ , >99.8%, Junsei). At 0 °C, 0.05 mol sodium hydroxide (NaOH, 97%, Junsei) was added into the above alcoholic solution with constant stirring. After about 30 min, virescent slurry formed, which was subsequently obturated in a 60 mL Teflon lined autoclave and kept at a constant temperature of 200 °C for 2 h in a regular laboratory oven. After the reaction systems cooled down, the products were washed by ethanol and water before being freeze-dried.

The crystal structure was determined with powder X-ray diffraction (XRD, Philips X'Pert-MPD system, Cu K $\alpha$  radiation,  $\lambda = 1.54056 \text{ \AA}$ ) at a scanning rate of 0.02° per s for  $2\theta$  in the range from 15° to 80°. The morphology and compositional information of the product materials was obtained with transmission electron microscopy (TEM, HITACHI, H-7500), high-resolution TEM, selected area electron diffraction (HRTEM/ED, JEOL, JEM-2010), field emission scanning electron microscopy, and energy-dispersive X-ray spectroscopy (FE-SEM/EDS, JEOL, JSM-6700FSEM). The magnetic proper-

\* Corresponding author. E-mail: yskang@pknu.ac.kr.

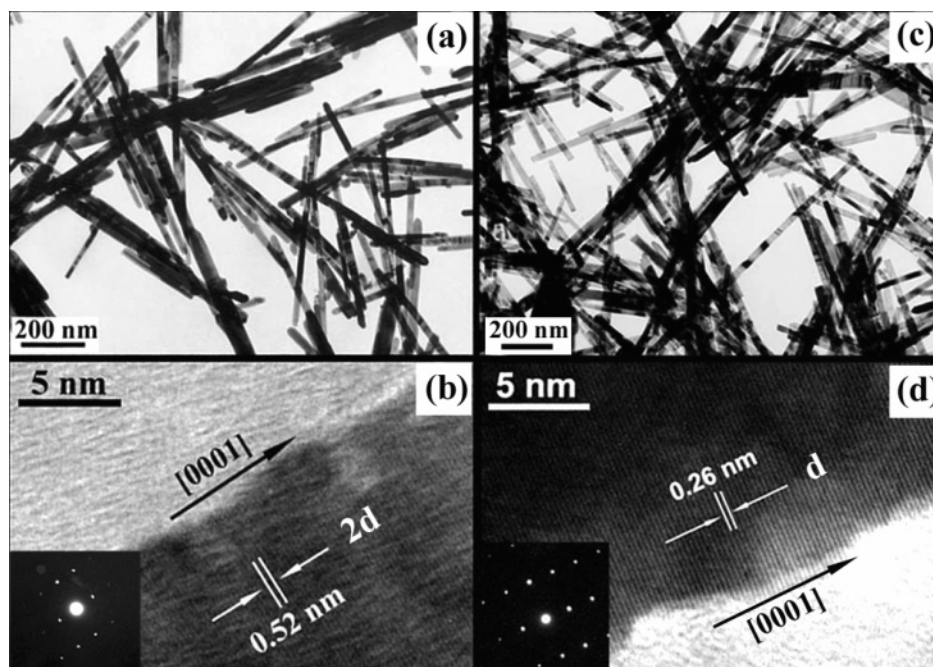


**Figure 1.** Electron microscopy characterization of the one-dimensional  $\text{Zn}_{1-x}\text{Ni}_x\text{O}$  solid solution and pure ZnO nanorods. (a) TEM image of  $\text{Zn}_{1-x}\text{Ni}_x\text{O}$  nanorods. (b) High-resolution TEM image of a single  $\text{Zn}_{1-x}\text{Ni}_x\text{O}$  nanorod, with an accompanying electron diffraction pattern in the inset; similar images for pure ZnO nanorods are shown in (c) and (d).

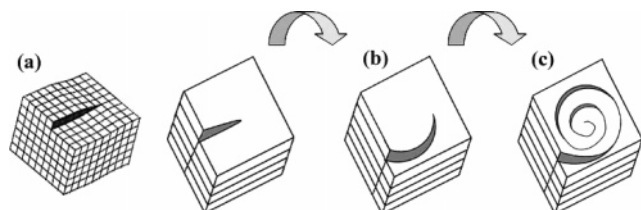


**Figure 2.** Screenshot dislocation model: (a) lattice defect, (b) and (c) propagation of screw.

ties of the obtained one-dimensional  $\text{Zn}_{1-x}\text{Ni}_x\text{O}$  solid solution samples were investigated with SQUID (Quantum Design MPMS XL7).

## Results and Discussion

The data of one-dimensional  $\text{Zn}_{1-x}\text{Ni}_x\text{O}$  solid solution presented below correspond to one specific synthesis, but the electron microscopy characterizations of the products diluted with different nickel concentration having small variations in average size were similar. The products were dispersed in ethanol by sonication to prepare samples for the measurements of TEM and SEM. Figure 1 shows transmission electron microscopy (TEM) and high-resolution TEM images of both  $\text{Zn}_{1-x}\text{Ni}_x\text{O}$  and pure ZnO nanorods. In Figure 1a, there are no visible defects, second phase, or precipitation in  $\text{Zn}_{1-x}\text{Ni}_x\text{O}$  nanorods compared with pure ZnO nanorods in Figure 1c. It

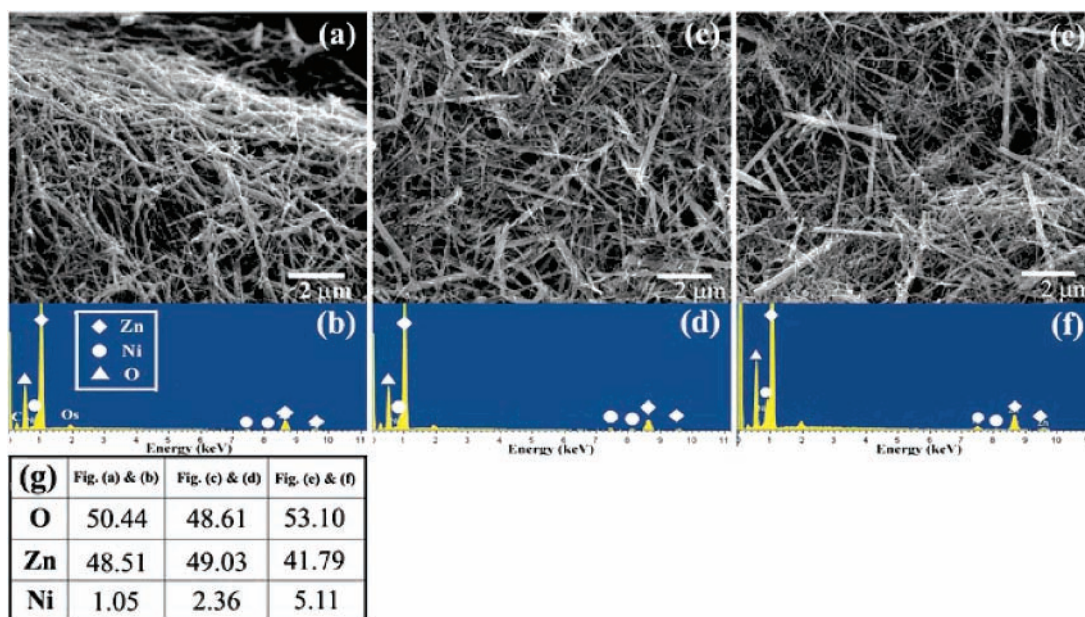


**Figure 3.** SEM images with the corresponding EDS spectra of  $\text{Zn}_{1-x}\text{Ni}_x\text{O}$  nanorods with a series of percentage of nickel dopant (in the reactants): (a) and (b) 2.5%, (c) and (d) 5%, (e) and (f) 10% nickel doping. (g) Quantitative elemental distribution in atomic percentage determined from EDS analysis.

suggests that the dopant is well integrated into the lattice sites during the alcoholysis process. The diameter of the nanorods is statistically invariant regardless of nickel concentration. The average diameter of  $\text{Zn}_{1-x}\text{Ni}_x\text{O}$  nanorods is 10–20 nm with length range from 0.2 to 1  $\mu\text{m}$ , thus the  $\text{Zn}_{1-x}\text{Ni}_x\text{O}$  nanorods have an aspect ratio range of 10–100. More detailed structure information of the ZnO-based nanorods was studied by high-resolution TEM (HRTEM) in conjunction with a selected area electron diffraction (SAED) pattern. The crystal lattice morphology of the nanorods has been examined by high-resolution TEM. Both of the lattice images in Figure 1b,d, recorded along the nanorods, clearly show the high crystallinity of the  $\text{Zn}_{1-x}\text{Ni}_x\text{O}$  and pure ZnO nanorods with no visible line or planar defects or amorphous shells on the surfaces of the nanorods. The insets of Figure 1b,d show the corresponding selected area electron diffraction (SAED) patterns from the same part of the nanorods shown in HR-TEM images (Figure 1b,d). The clear linearly arranged patterns confirm that the  $\text{Zn}_{1-x}\text{Ni}_x\text{O}$  nanorod has the wurtzite structure, and there is no formation of nickel precipitated as a secondary phase. From the HR-TEM images and SAED patterns, it is seen that both kinds of rods are single crystalline, with a growth direction along the  $c$ -axis (indexes the [0001] direction).

One-dimensional growth of pure ZnO nanorods has been reported previously in alcoholic solutions.<sup>1d</sup> In the reported process, the one-dimensional growth was enabled by the screw dislocation model of crystal growth, which can be simply presented in Figure 2. At the nucleation stage, the low-energy facets such as the nonpolar facets {01-10} and polar facets (0002) in wurtzite structure have the preference to be formed first.<sup>12</sup> The kink site (for example, lattice defects, etc.) of the nuclei with the highest binding energy is the most favorable position for the incorporation of a unit molecule from the solution phase, and the angular velocity near the corner of the lattice defects is faster than that at the edge of the crystal. Thus, the dislocation proceeds in a spiral form in the propagation of the step, which results in the smooth side facets of the crystals. Finally, the extending of the smooth low-energy side facets, the {01-10} facets of wurtzite structure, lead the oriented growth into one-dimensional forms.<sup>1d,13</sup> It is believed that the screw dislocation model plays the similar role in fabrication of  $\text{Zn}_{1-x}\text{Ni}_x\text{O}$  nanorods here, which formed the uniform diameters and single crystalline structures of the  $\text{Zn}_{1-x}\text{Ni}_x\text{O}$  nanorods along their entire length on the  $c$ -axis (the [0001] growth direction).

Figure 3 shows SEM images and the corresponding energy dispersive X-ray spectroscopy (EDS) of  $\text{Zn}_{1-x}\text{Ni}_x\text{O}$  nanorods with various levels of nickel doping. The EDS spectra from parts a, c, and e of Figure 3 are correspondingly displayed in parts b, d, and f of Figure 3, respectively, and the quantitative elemental distribution in atomic percentage is presented as the table in Figure 3g. With consideration of the accuracy of the EDS analysis, we can conclude that there are ~2.1%, ~4.6%, and ~10.9% atomic ratios of nickel doping in the ZnO nanorods, respectively, corresponding with the series levels of nickel acetate ranging from 2.5% to 5% and 10% in the reactants. The difference of nickel concentration between reactants and products is possibly caused by the formation of small oxide clusters of both ZnO and NiO, which did not precipitate out or, alternatively, the different dissolution ratios between ZnO and NiO clusters. Both of which were discarded in the purification steps.

Powder X-ray diffraction was used to characterize the structure of the products. Typical XRD patterns of  $\text{Zn}_{1-x}\text{Ni}_x\text{O}$  nanorods with various levels of nickel doping are presented in

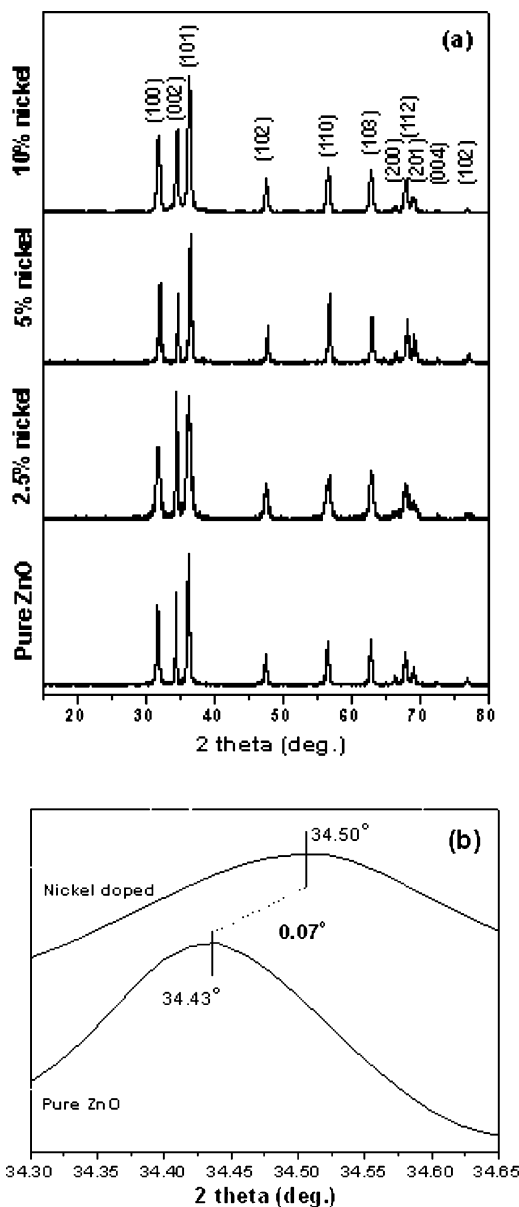


**Figure 4.** Compared XRD patterns of pure ZnO nanorods and  $\text{Zn}_{1-x}\text{Ni}_x\text{O}$  nanorods with a series of percentage of nickel dopant (in the reactants). (a) Full angle range of XRD patterns. (b) High-resolution of (002) peak.

Figure 4. In all cases, wurtzite is the only phase in existence that indicates the possible uniform doping throughout the nanorods. It should be noted that, even though no nickel clusters or other secondary phases were observed under the resolution limit of XRD, their existence cannot be completely excluded. However, the microstructure of the  $\text{Zn}_{1-x}\text{Ni}_x\text{O}$  nanorods was examined by high-resolution TEM, and all images show that the surfaces of the  $\text{Zn}_{1-x}\text{Ni}_x\text{O}$  nanorods are rather smooth and clean and the lattice is uniform throughout their entire lengths. Thus, nickel ions were uniformly doped into wurtzite ZnO by replacing the zinc sites. The small difference between the ionic radii of the tetrahedrally coordinated zinc(II) (0.74 Å) and the nickel(II) (0.69 Å) allows incorporation of  $\text{Ni}^{2+}$  into ZnO with only slight decrease in lattice parameters that cause a shift of the ZnO (002) peak to a higher angle by about 0.07° (as shown in Figure 4b). The similar phenomenon, ZnO (002) peaks shifted to a lower angle due to the difference between the ionic radii of the tetrahedrally coordinated Mn(II) (0.80 Å) and Zn(II), was reported in Mn-doped ZnO nanowire by Lee et al.<sup>7b</sup>

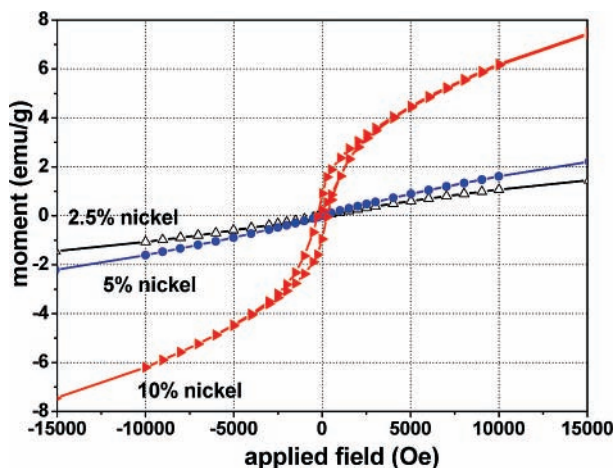


**Figure 5.** Magnetization (300 K) of  $\text{Zn}_{1-x}\text{Ni}_x\text{O}$  nanorods with a series of percentage of nickel dopant (in the reactants).

The magnetic properties of the  $\text{Zn}_{1-x}\text{Ni}_x\text{O}$  nanorods with various nickel doping levels were investigated on a SQUID magnetometer. Figure 5 shows the magnetization ( $M$ ) vs magnetic field ( $H$ ) measured at 300 K. The diamagnetic background of the sapphire substrate has been subtracted. Whereas paramagnetism dominates the magnetism of the  $\text{Zn}_{1-x}\text{Ni}_x\text{O}$  nanorods with low nickel doping levels, which results in little detectable magnetization at 300 K, a clear hysteresis loop is observed in the  $\sim 10\%$  of nickel doped  $\text{Zn}_{1-x}\text{Ni}_x\text{O}$  nanorods with a 300 K coercivity ( $H_c$ ) of 259 Oe. It demonstrates that room-temperature ferromagnetic ordering exists in the one-dimensional ZnO solid solution with nickel solute. The physical origin of the ferromagnetic ordering from the dilute magnetic semiconductors is under discussion as to whether the ferromagnetism arises from the homogeneous magnetic doping or from magnetic precipitation.<sup>14</sup> In our case, the single-phased XRD patterns, the slightly shifted ZnO (002) peak with nickel doping, the well aligned lattice without any lattice distortion, and no nanoscale phases have been observed in high-resolution TEM images. These confirm that nickel occupies zinc sites in  $\text{Zn}_{1-x}\text{Ni}_x\text{O}$  nanorods. Therefore, the detected ferromagnetism here arises from the homogeneous doping of nickel into ZnO crystal formed solid solutions.

## Conclusion

In conclusion, ZnO-based solid solutions with different nickel concentration levels were synthesized via a non-surfactant-assisted solvothermal method. The  $\text{Zn}_{1-x}\text{Ni}_x\text{O}$  nanorods show ferromagnetic properties at room temperature. The structure analysis indicated that the  $\text{Zn}_{1-x}\text{Ni}_x\text{O}$  nanorods are single crystalline. This suggests that the solid solution of nickel ions

in ZnO nanorods plays a major role in producing the detected ferromagnetic behaviors. These  $\text{Zn}_{1-x}\text{Ni}_x\text{O}$  nanorods offer applications in fundamental science and future nanoscale spintronic devices. Moreover, the economical and facile method presented here can be potentially applied in wide range of one-dimensional dilute magnetic semiconductors.

**Acknowledgment.** This work is financially supported by the Brain Korea 21 program and Functional Chemicals Development Program.

## References and Notes

- (1) (a) Huang, M. H.; Mao, S.; Feick, H.; Yan, H.; Wu, Y.; Kind, H.; Weber, E.; Russo, R.; Yang, P. D. *Science* **2001**, *292*, 1897. (b) Wang, Z. L.; Song, J. H. *Science* **2006**, *312*, 242. (c) Minne, S. C.; Manalis, S. R.; Quate, C. F. *Appl. Phys. Lett.* **1995**, *67*, 3918. (d) Zhang, X. L.; Kang, Y. S. *Inorg. Chem.* **2006**, *45*, 4186.
- (2) (a) Choi, H. J.; Seong, H. K.; Chang, J. Y.; Lee, K.; Park, Y. J.; Kim, J. J.; Lee, S. K.; He, R. R.; Kuykendall, T.; Yang, P. D. *Adv. Mater.* **2005**, *17*, 1351. (b) Zheng, G. F.; Lu, W.; Jin, S.; Lieber, C. M. *Adv. Mater.* **2004**, *16*, 1890.
- (3) (a) Ohno, H. *Science* **1998**, *281*, 951. (b) Dietl, T.; Ohno, H.; Matsukura, F.; Cibert, J.; Ferrand, D. *Science* **2000**, *287*, 1019. (c) Archer, P. I.; Redovanovic, P. V.; Heald, S. M.; Gamelin, D. R. *J. Am. Chem. Soc.* **2005**, *127*, 14479. (d) Pan, D.; Wan, J.; Xu, G.; Lv, L.; Wu, Y.; Min, H.; Liu, J.; Wang, G. *J. Am. Chem. Soc.* **2006**, *128*, 12608.
- (4) Sato, K.; Katayama-Yoshida, H. *Phys. E* **2001**, *10*, 251.
- (5) (a) Chang, Y. Q.; Wang, D. B.; Luo, X. H.; Xu, X. Y.; Chen, X. H.; Li, L.; Chen, C. P.; Wang, R. M.; Yu, D. P. *Appl. Phys. Lett.* **2003**, *83*, 4020. (b) Pan, Z. W.; Wang, Z. L. *Science* **2001**, *291*, 1947.
- (6) (a) Sharma, P.; Gupta, A.; Rao, K. V.; Owens, F. J.; Sharma, R.; Ahuja, R.; Guillen, J. M. O.; Johansson, B.; Gehring, G. A. *Nat. Mater.* **2003**, *2*, 673. (b) Zhu, T.; Zhan, W. S.; Wang, W. G.; Xiao, J. Q. *Appl. Phys. Lett.* **2006**, *89*, 022508. (c) Nakayama, M.; Tanaka, H.; Masuko, K.; Fukushima, T.; Ashida, A.; Fujimura, N. *Appl. Phys. Lett.* **2006**, *88*, 241908. (d) Zhang, Y. B.; Liu, Q.; Sriharan, T.; Gan, C. L.; Li, S. *Appl. Phys. Lett.* **2006**, *89*, 042510. (e) Radovanovic, P. V.; Norberg, N. S.; McNally, K. E.; Gamelin, D. R. *J. Am. Chem. Soc.* **2002**, *124*, 15192. (f) Meron, T.; Markovich, G. *J. Phys. Chem. B* **2005**, *109*, 20232. (g) Deka, S.; Pasricha, P.; Joy, P. A. *Chem. Mater.* **2004**, *16*, 1168.
- (7) (a) He, J. H.; Lao, C. B.; Chen, L. J.; Davidovic, D.; Wang, Z. L. *J. Am. Chem. Soc.* **2005**, *127*, 16376. (b) Baik, J. M.; Lee, J. L. *Adv. Mater.* **2005**, *17*, 2745. (c) Liu, L. Q.; Xiang, B.; Zhang, X. Z.; Zhang, Y.; Yu, D. P. *Appl. Phys. Lett.* **2006**, *88*, 063104. (d) Philipose, U.; Nair, S. V.; Trudel, S.; de Souza, C. F.; Aouba, S.; Hill, R. H.; Ruda, H. E. *Appl. Phys. Lett.* **2006**, *88*, 263101.
- (8) Wu, J. J.; Liu, S. C.; Wang, M. H. *Appl. Phys. Lett.* **2004**, *85*, 1027.
- (9) (a) Schwartz, D. A.; Norberg, N. S.; Nguyen, Q. P.; Parker, J. M.; Gamelin, D. R. *J. Am. Chem. Soc.* **2003**, *125*, 13205. (b) Schwartz, D. A.; Kittilstved, K. R.; Gamelin, D. R. *Appl. Phys. Lett.* **2004**, *85*, 1395.
- (10) Yuhas, B. D.; Zitoun, D. O.; Pauzuskie, P. J.; He, R.; Yang, P. *Angew. Chem., Int. Ed.* **2006**, *45*, 420.
- (11) Wang, H.; Wang, H. B.; Yang, F. J.; Chen, Y.; Zhang, C.; Yang, C. P.; Li, Q.; Wong, S. P. *Nanotechnology* **2006**, *17*, 4312.
- (12) Wang, Z. L. *J. Phys.: Condens. Matter* **2004**, *16*, R829.
- (13) Ohtaki, H. *Crystallization Processes*; John Wiley & Sons Ltd: Chichester, U.K., 1998.
- (14) Park, J. H.; Kim, M. G.; Jang, H. M.; Ryu, S. *Appl. Phys. Lett.* **2004**, *84*, 1338.